

# Photo Gel–Sol/Sol–Gel Transition and Its Patterning of a Supramolecular Hydrogel as Stimuli-Responsive Biomaterials

Shinji Matsumoto,<sup>[a]</sup> Satoshi Yamaguchi,<sup>[b]</sup> Shiori Ueno,<sup>[a]</sup> Harunobu Komatsu,<sup>[a]</sup> Masato Ikeda,<sup>[a]</sup> Koji Ishizuka,<sup>[c]</sup> Yuko Iko,<sup>[c]</sup> Kazuhito V. Tabata,<sup>[c]</sup> Hiroyuki Aoki,<sup>[d]</sup> Shinzaburo Ito,<sup>[d]</sup> Hiroyuki Noji,<sup>[c]</sup> and Itaru Hamachi\*<sup>[a, b]</sup>

**Abstract:** In a focused library of glycolipid-based hydrogelators bearing fumaric amide as a *trans–cis* photoswitching module, several new photoresponsive supramolecular hydrogelators were discovered, the gel–sol/sol–gel transition of which was pseudo-reversibly induced by light. Studying the optimal hydrogel by NMR spectroscopy and various microscopy techniques showed that the *trans–cis* photoisomerization of the double bond of the fumaric amide unit effectively caused assembly or disassembly of the self-assembled supramolecular fibers to yield the macroscopic hydrogel or the corresponding sol, respectively. The entanglement of the supramolecular fibers produced nanomeshes, the void space

of which was roughly evaluated to be 250 nm based on confocal laser scanning microscopy observations of the size-dependent Brownian motion of nanobeads embedded in the supramolecular hydrogel. It was clearly shown that such nanomeshes become a physical obstacle that captures submicro- to micrometer-sized substrates such as beads or bacteria. By exploiting the photoresponsive property of the supramolecular nanomeshes, we succeeded in off/on switching of bacterial movement and rotary motion of bead-

tethered F<sub>1</sub>-ATPase, a biomolecular motor protein, in the supramolecular hydrogel. Furthermore, by using the photolithographic technique, gel–sol photopatterning was successfully conducted to produce sol spots within the gel matrix. The fabricated gel–sol pattern not only allowed regulation of bacterial motility in a limited area, but also off/on switching of F<sub>1</sub>-ATPase rotary motion at the single-molecule level. These results demonstrated that the photoresponsive supramolecular hydrogel and the resulting nanomeshes may provide unique biomaterials for the spatiotemporal manipulation of various biomolecules and live bacteria.

**Keywords:** gels · immobilization · photochemistry · self-assembly · supramolecular chemistry

## Introduction

For advances in nanobiotechnology and nanomedicine, sophisticated devices<sup>[1]</sup> and materials<sup>[2]</sup> capable of manipulating the function, activity, or mobility of biomacromolecules such as DNA, proteins, organelles, and cells are crucial. To develop such intelligent biodevices, the bottom-up approach is now considered to be complimentary to the top-down approach, so their rational combination should be promising. Among the bottom-up approaches for well-organized structures and functions, a supramolecular strategy in which molecular self-assembly based on weak noncovalent interactions is effectively utilized seems promising. For example, supramolecular hydrogels<sup>[3]</sup> are attractive biomaterials not only because they can entrap various biomolecules without denaturation, but also because they form hierarchical molecular assemblies in which flexible nanofibers with high aspect ratio are constructed into 3D fiber networks with sizes rang-

[a] S. Matsumoto, S. Ueno, H. Komatsu, Dr. M. Ikeda, Prof. Dr. I. Hamachi  
Department of Synthetic Chemistry and Biological Chemistry  
Kyoto University  
Katsura, Nishikyo-Ku, Kyoto, 615–8510 (Japan)  
Fax: (+81)75-383-2759  
E-mail: ihamachi@sbchem.kyoto-u.ac.jp

[b] Dr. S. Yamaguchi, Prof. Dr. I. Hamachi  
PRESTO (Synthesis and Control, JST) (Japan)

[c] K. Ishizuka, Y. Iko, Dr. K. V. Tabata, Prof. Dr. H. Noji  
ISIR, Osaka University  
8-1 Mihogaoka, Ibaraki, Osaka, 567-0047 (Japan)

[d] Dr. H. Aoki, Prof. Dr. S. Ito  
Department of Polymer Chemistry, Kyoto University  
Katsura, Nishikyo-Ku, Kyoto, 615-8510 (Japan)

Supporting information for this article is available on the WWW under <http://www.chemeurj.org/> or from the author.

ing from submicrometer to hundreds of micrometers and finally to macroscopic hydrogels with millimeter size.<sup>[4,5,10d]</sup> This hierarchy provides the valuable characteristic that subtle structural changes in the constituent elements can directly influence the macroscopic properties of the supramolecular materials. Due to such benefits, a growing number of intelligent supramolecular hydrogels that respond to thermal,<sup>[3]</sup> pH,<sup>[6]</sup> enzyme<sup>[7]</sup> and other stimuli<sup>[8]</sup> have recently emerged. In these examples, a stimulus-responsive module was incorporated into a small molecule as an element of the corresponding supramolecule to induce a macroscopic change in the self-assembled hydrogel.

Among these stimuli, light is unique in that remote input in a spatially and temporally controlled manner is readily accomplished. Thus, photostimuli are expected to be highly useful, especially for the fabrication of supramolecular materials.<sup>[9]</sup> However, photoresponsive supramolecular hydrogels<sup>[10]</sup> are poorly developed in comparison to the many examples of photodriven molecular machines and molecular switching.<sup>[11]</sup> We now describe a strategy that couples partially rational design with a focused combinatorial library and provides a powerful method for the discovery of novel photoresponsive supramolecular hydrogels. In addition to conventional structural analysis, the mesh size of the formed supramolecular fibers was examined in terms of substrate release and direct observation of the Brownian motion of nanobeads embedded in the hydrogel, both of which were found to be photoregulated. By exploiting the photoinduced gel-to-sol phase transition of the supramolecular hydrogel, photo gel-sol patterning was also successfully accomplished, and thus rotational movement of the microbead-tethered  $F_1$ -ATPase, a biological motor protein, and bacterial motility were spatially and temporally controlled.

## Results and Discussion

**Molecular design and synthesis:** We recently reported a detailed structural analysis of glycolipid-based supramolecular hydrogel **1** (Figure 1 a), which suggested that well-developed hydrogen-bonding (H-B) networks in the spacer region cooperatively contribute to stabilization of the supramolecular gel fibers, together with van der Waals packing of the tail modules and water-mediated intermolecular hydrogen-bond-

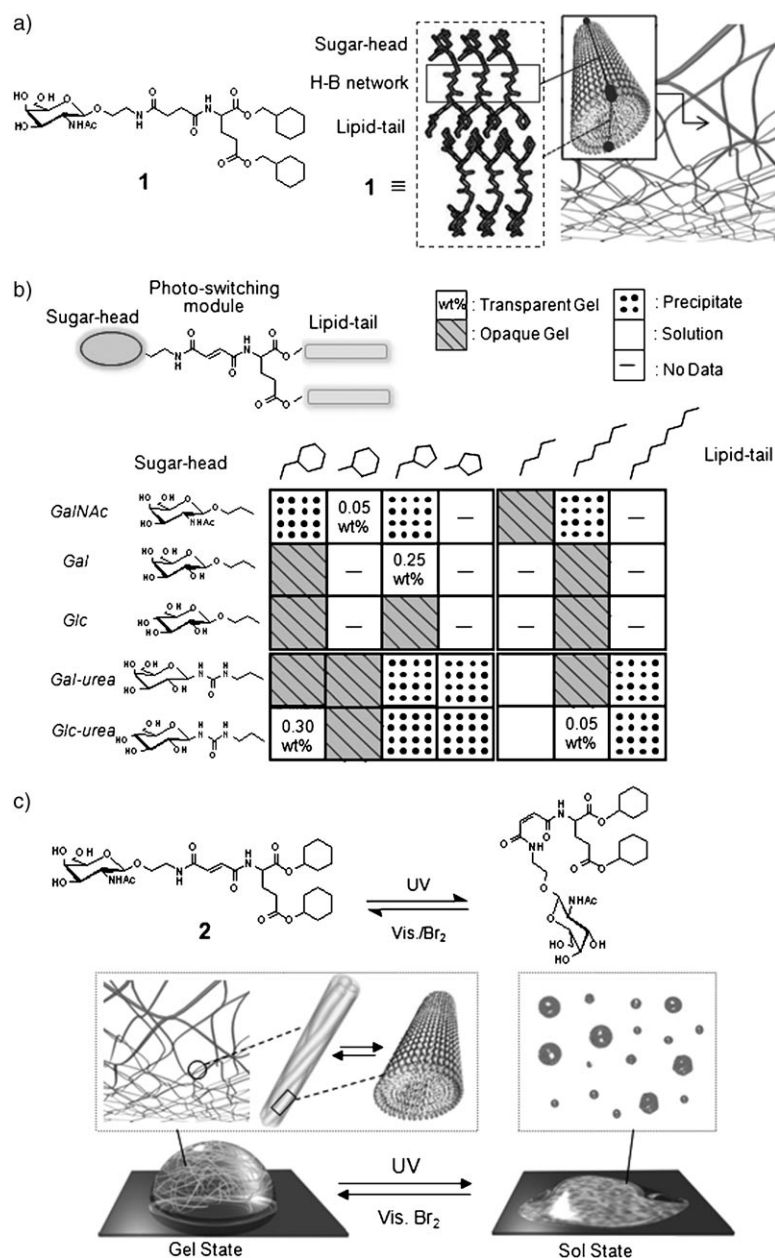


Figure 1. Structure of glycolipid-based supramolecular hydrogelators. a) Chemical structure of hydrogelator **1** and molecular packing of gel fibers of **1**. b) A small library for screening photoresponsive hydrogelators. Hydrophilic sugar-head (column) and hydrophobic lipid-tail (rows) modules were altered. The gelation test results were classified into transparent gel, opaque gel, precipitate, and homogenous solution, as shown in the table. c) Scheme of *trans/cis* photoisomerization of **2** and a schematic illustration of the pseudoreversible gel-sol transition of hydrogel **2** induced by UV/Vis irradiation.

ing linking the saccharide heads.<sup>[4a]</sup> On the basis of these structural features, we decided to incorporate a photoswitching module into the spacer unit of the gelator in order to induce disassembly and/or assembly of the central hydrogen-bonding network. The subtle change caused by isomerization of the module in the assembled element was expected to induce the macroscopic gel–sol and/or sol–gel transition of the supramolecular hydrogel. In practice, with retention of the other structural modules, the succinic amide spacer of gelator **1** was replaced with fumaric amide as a photoresponsive module which can undergo photoisomerization to the maleic amide. It seemed reasonable to assume that the H-B network is retained in the *trans* conformation (fumaric amide) without any strain because of the structural similarity to the succinic amide, whereas it may be partially disrupted in the *cis* conformation (maleic amide). Unfortunately, however, the simple replacement of succinic amide with fumaric amide led to loss of gelation capability. Thus, we prepared a small combinatorial library of relevant derivatives by changing other modules, such as the sugar head and the hydrophobic tail, from which several low molecular weight hydrogelators were discovered (Figure 1b). Molecules consisting of a GalNAc head and cyclohexyl tails or a Gal head and methylcyclopentyl tails formed stable and transparent hydrogels. Among the molecules bearing a urea unit between the spacer module and the sugar head, we found that Glc-urea/methylcyclohexyl and Glc-urea/*n*-hexyl formed stable hydrogels. In particular, gelator **2** (Figure 1c) displayed superior hydrogelation properties, in that a transparent hydrogel formed at a low concentration (0.05 wt% of the critical gelation concentration). Figure 2b shows the dependence of the storage ( $G'$ ) and loss ( $G''$ ) moduli of hydrogel **2** on the angular frequency ( $\omega$ ), as measured by a rheometer. The appearance of a plateau for  $G'$

and  $G''$  at 100–0.10  $\text{rad s}^{-1}$  clearly indicated that the hydrogelator **2** forms a rheologically stable gel.

**Photoinduced gel-to-sol and/or sol-to-gel transition:** As shown in Figure 2a, UV irradiation of the hydrogel of **2** produced a fluid sol state with a concurrent increase in transparency. Based on dynamic viscoelasticity measurements on the fluid sol (Figure 2b), we found that  $G'$  at 0.10  $\text{rad s}^{-1}$  became 10<sup>5</sup>-fold smaller than in the initial gel state and both

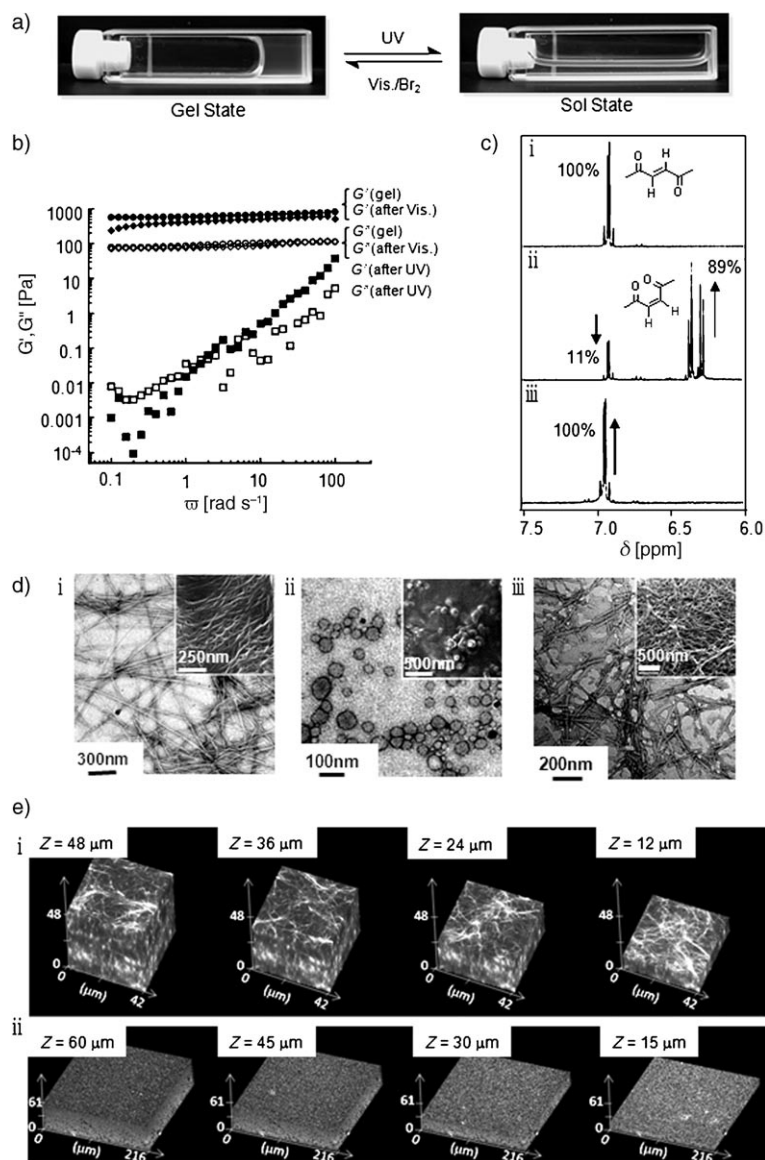


Figure 2. Pseudoreversible photo gel–sol transition of hydrogel **2**. a) Photographs of hydrogel **2** before and after UV or Vis ( $\text{Br}_2$ ) irradiation. b) Dynamic viscoelastic properties of hydrogel **2**, the sol after UV irradiation of gel **2**, and the reconstructed gel **2** after Vis ( $\text{Br}_2$ ) irradiation to give the sol.  $G'$  (●: before UV, ■: after UV, ▲: after Vis),  $G''$  (○: before UV, □: after UV, △: after Vis). c) Enlarged  $^1\text{H}$  NMR spectra of i) the gel state of **2**, ii) the sol state after UV irradiation for 30 min, and iii) the regelated sample after Vis ( $\text{Br}_2$ ) irradiation for 10 min. d) TEM and SEM (inset) images of i) gel **2** before UV irradiation, ii) sol state after UV irradiation of the gel, and iii) reconstructed gel after Vis ( $\text{Br}_2$ ) irradiation of the sol. e) 3D CLSM fluorescence images of hydrogel **2** stained with a hydrophobic fluorescent rhodamine dye ( $[\text{C}_{18}\text{-Rho}] = 25 \mu\text{M}$ , excitation wavelength 543 nm). Hydrogel **2** before (i) and after UV irradiation (ii). See the Supporting Information for color version of Figure 2e.

$G'$  and  $G''$  drastically decreased in dependence on the angular frequency. This rheological behavior showed that a typical gel–sol phase transition occurred on UV irradiation. The  $^1\text{H}$  NMR studies on the sol state indicated that 89% of the fumaric (*trans*) form was converted to the maleic (*cis*) form (Figure 2c). The gel-to-sol transition is dependent on the *trans/cis* isomerization ratio, and a threshold content of at least 50% of the *cis* form is needed for the gel–sol transition (see Figure S1 in the Supporting Information). Transmission and scanning electron microscopy (TEM, SEM) provided insight into the morphology of the self-assembled gel fibers (Figure 2d). In the gel state, many fibers having a length greater than 10  $\mu\text{m}$  and a width of less than 20 nm are entangled in a manner similar to other supramolecular hydrogels (see Figure S2 in the Supporting Information), whereas only spherical aggregates such as vesicles, instead of the entangled fibers, were observed in the sol state (Figure 2d). It is reasonably assumed that such spherical aggregates are not capable of entangling each other, so that a loss of cross-linking points essential for gel formation resulted in the destruction of the macroscopic hydrogel. Confocal laser scanning microscopy (CLSM) observations directly produced a 3D image of the hydrogel (see Figure 2e and see Figure S3 in the Supporting Information). For this method, we did not need to dry the gel sample; instead, the gel-fiber domain was stained with a fluorescent and hydrophobic rhodamine probe (octadecyl rhodamine B chloride:  $\text{C}_{18}\text{-Rho}$ ) in the wet gel state. Depth profiling clearly revealed the well-entangled 3D network (so-called supramolecular mesh) of fibers in the gel state, whereas the fibrous network disappeared after the photoirradiation. Powder X-ray diffraction (XRD) measurements on the gel showed two main peaks at  $2.15^\circ$  (41 Å) and  $20.7^\circ$  (4.3 Å; see Figure S4 in the Supporting Information), the pattern of which is almost identical to that of succinic-amide-type gelator **1**.<sup>[4a]</sup> Based on previous studies, the small-angle peak is assigned to the tilted bimolecular length of **2**, and the wide-angle peak corresponds to the packed thickness of the cyclohexyl ring. On the other hand, significant broadening of these two peaks in the sample prepared from the sol state suggests that the regular packing structure is significantly disturbed by the photoinduced *trans*-to-*cis* conformational change.

Interestingly, reconstruction of the hydrogel from the sol state prepared by visible-light irradiation was successful. Visible-light irradiation of the fluid sol of **2** afforded the stable hydrogel in the presence of a small amount of bromine. The rheological behavior of the reconstructed hydrogel was similar to that of the initial gel state (Figure 2b), that is, both  $G'$  and  $G''$  showed a plateau versus angular frequency, and  $G'$  at 0.10  $\text{rad s}^{-1}$  was almost  $10^5$  greater than in the sol state. This gel-to-sol and sol-to gel cycle was repeated several times.  $^1\text{H}$  NMR spectroscopy confirmed that *cis* (maleic amide) to *trans* (fumaric amide) isomerization occurred in 100% yield without any serious side reactions (Figure 2c). Morphological studies by TEM and SEM showed regeneration of well-developed fibrous networks that are indistinguishable from the original (Figure 2d).

These results suggest that the *cis*-to-*trans* photoisomerization repaired the tight packing of self-assembled **2**, so that the regenerated long fibers facilitated formation of the hydrogel. Thus, macroscopic gel–sol and sol–gel transition are pseudo-reversibly photocontrolled by the molecular-level conformational change in the present supramolecular hydrogel (Figure 1c).

#### Photocontrolled substrate release by photoresponsive hydrogel:

The supramolecular fibrous network of the gel is capable of immobilizing various substrates. Using the photoresponsive gel–sol transition of hydrogel **2**, we next attempted photocontrolled substrate release. Water-soluble vitamin  $\text{B}_{12}$  ( $\text{B}_{12}$ ) entrapped in supramolecular hydrogel **2** was slowly released from the gel into the bulk aqueous solution over a period longer than 10 h (7.8% of the embedded  $\text{B}_{12}$  was released in the initial 3 h; Figure 3a). On the other

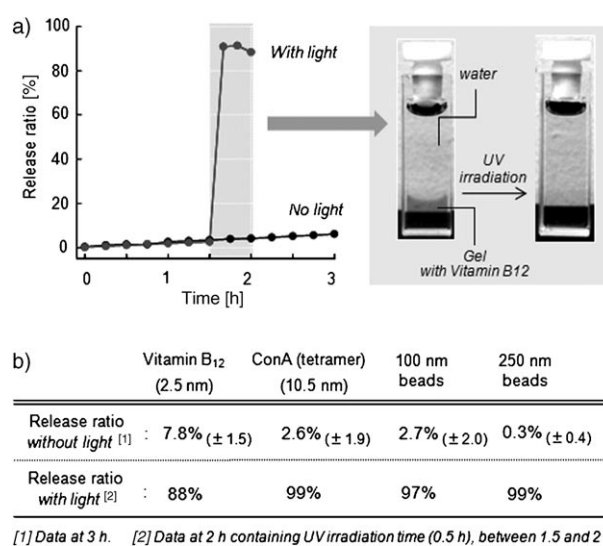


Figure 3. Release of biomolecules and microbeads by photoresponsive gel–sol transition. a) Photocontrolled release of vitamin  $\text{B}_{12}$  from hydrogel **2**. Time courses of release ratio [%] of vitamin  $\text{B}_{12}$  from gel to bulk solution without or with UV irradiation [filled black circles: spontaneous release; filled gray circles: phototriggered release (irradiation at 1.5 h)]. b) Release ratio [%] of vitamin  $\text{B}_{12}$ , FITC-ConA, and 100 and 250 nm fluorescent beads from hydrogel **2** without or with UV irradiation. See the Supporting Information for color version of Figure 3a.

hand, rapid release of  $\text{B}_{12}$  took place on UV-induced gel-to-sol transition (almost 100% in 10 min). Similarly, glucose-binding protein Con A, as well as nanobeads with diameters of 100 or 250 nm, which were entrapped in gel **2** were released by photoinduced gel-to-sol transition with almost the same efficiency as  $\text{B}_{12}$  (Figure 3b).

Interestingly, the rate of substrate release without UV light depends on the substrate size. For vitamin  $\text{B}_{12}$ , which is about 2.5 nm in diameter, 7.8% was released in the first 3 h, whereas both Con A (10.5 nm diameter) and the 100 nm beads showed only about 2.6% release in 3 h. Release was almost completely suppressed (about 0% in 3 h) in the case of the 250 nm beads. These results indicate that the present

supramolecular hydrogel can act as a barrier against the release of substrates of various sizes with efficiencies that depend on substrate size, and the barrier capability can be photomodulated regardless of substrate size.

#### Evaluation of the size of meshes composed of photoresponsive hydrogel:

A CLSM study on the Brownian motion of fluorescent nanobeads in the gel matrix gave further insights into understanding how the supramolecular hydrogel can entrap these substrates in the inner space.<sup>[12]</sup> We can directly observe the motion of fluorescent beads by CLSM. In the case of beads with a diameter of 100 nm, smooth diffusion occurred inside hydrogel **2** (0.10 wt %), so that a static image was difficult to obtain (Figure 4a). In contrast, all the beads with a diameter of 250 nm stopped in the gel matrix (Figure 4b). Perfect stopping was also observed for 500 and 1000 nm beads (see Figure 4c and Figure S5 in the Supporting Information). Thus, we achieved 3D spatial fixation of these beads in the CLSM image. Moving or stopping of the

Brownian motion of the nanobeads showed a critical threshold bead size. This suggests that the present supramolecular hydrogel formed nanomeshes with relatively homogeneous void spaces of between 100 and 250 nm, which are strong enough to function as a physical obstacle to trap the beads. As shown Figure 4c, by increasing the gelator concentration to 0.30 wt %, the motion of even the 100 nm beads is perfectly stopped. Below the critical gelation concentration (cgc) of 0.035 wt % (sol state), on the other hand, no beads of any size stopped, probably due to the insufficient development or entanglement of the fibers to form well-developed meshes. Between 0.05 (cgc) and 0.20 wt %, the threshold (100–250 nm) was not substantially affected. These results imply that the mesh size of the supramolecular hydrogel was dependent on gelator concentration.

It is also noteworthy that the present method is much simpler and more general for directly evaluating the mesh size of intact hydrogels without drying than the method using nanobead-tethered F<sub>1</sub>-ATPase that was recently reported by us.<sup>[13]</sup>

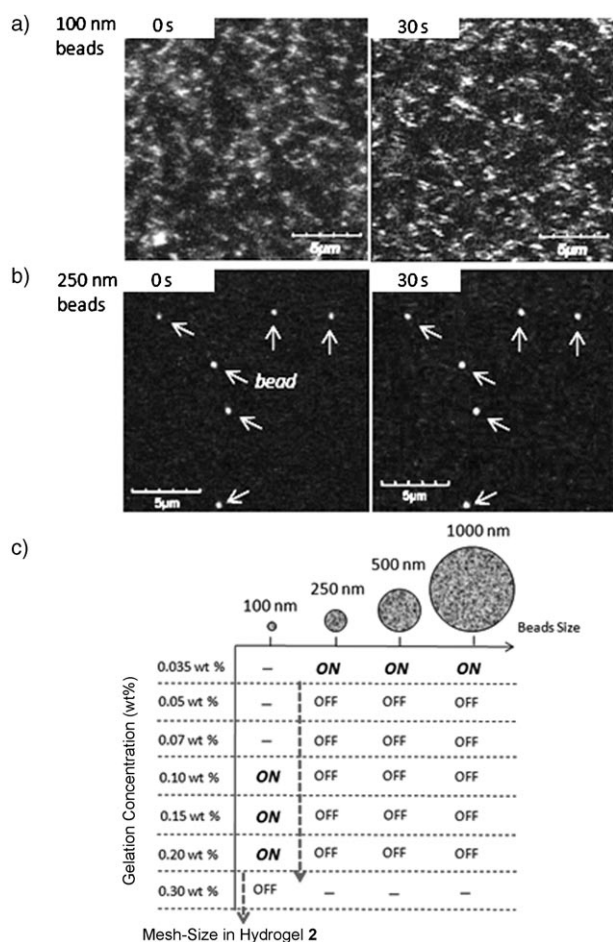


Figure 4. Time-dependent CLSM images for the analysis of Brownian motion of hydrophilic microbeads in hydrogel **2** (0.10 wt % in ion-exchanged water). a) 100 and b) 250 nm beads stained by rhodamine dye. c) Summary of the Brownian motions of 100–1000 nm beads in hydrogel **2**. ON and OFF mean starting and stopping of Brownian motion of the microbeads, respectively. See Supporting Information for color version of Figure 4a,b.

#### Off/on switching of bacterial movement and rotation of F<sub>1</sub>-ATPase motor by means of photoresponsive supramolecular nanomeshes:

Like the nanobeads, the movement of living *E. coli* bacteria (EGFP-BL21) can be photocontrolled by the supramolecular meshes, because their size is within the micrometer range, slightly larger than the 250 nm beads. For the direct detection of both the bacteria and the gel fibers, green fluorescent bacteria overexpressing enhanced green fluorescent protein (EGFP) and red fluorescent fibers stained with C<sub>18</sub>-Rho were used. Using the CLSM method we observed free movement of the bacteria in the sol state of **2** in a flow-cell chamber and stopping of the movement by the gel formation, similar to the nanobeads (Figure 5a–c). On the other hand, bacterial movement restarted together with disappearance of the gel meshes after UV irradiation of the gel matrix for 30 s. Careful CLSM observations of bacteria embedded in hydrogel **2** showed that many bacteria were entangled within the supramolecular meshes (Figure 5a), and this suggests that the gel-fiber meshes can act as an efficient physical obstacle against bacterial movement (Figure 5d).

In addition to bacteria, photoinduced off/on switching of enzymatic motion was successfully conducted when the nanobeads were attached to the enzyme. In a proof-of-concept experiment, we examined the motion of F<sub>1</sub>-ATPase, an enzyme-based molecular motor, by microscopy. After tethering submicrometer-beads (normally 0.73 μm in diameter) to F<sub>1</sub>-ATPase, we observed the rotary motion of the microbead-appended F<sub>1</sub>-ATPase by following the motion of the beads at the single-molecule level.<sup>[13,14]</sup> The rotary motion of the microbead-tethered F<sub>1</sub>-ATPase stopped concurrently with gel formation in the cell chamber after infusion of the sol state of **2** (see Figure S6 in the Supporting Information). Interestingly, after 1.5–3.5 min of UV irradiation by a low-pressure Hg lamp, F<sub>1</sub>-ATPase rotation restarted along with the photoinduced gel-to-sol transition of **2** (see Figure S6 in

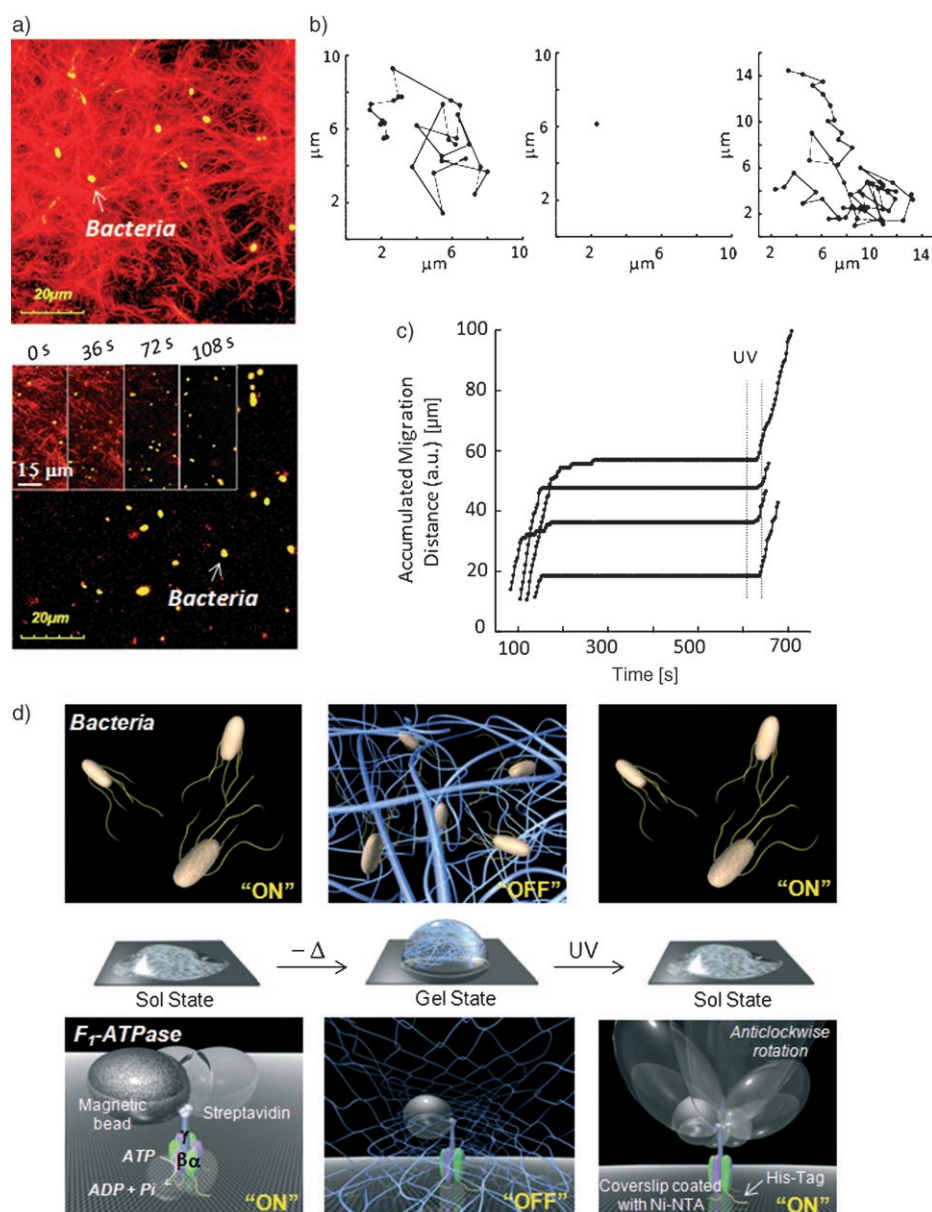


Figure 5. Off/on switching of *E. coli* (BL21). Bacterial movement and rotation of microbead-tethered F<sub>1</sub>-ATPase were controlled by using the photoresponsive supramolecular meshes of **2**. a) CLSM observation of *E. coli*. (BL21) overexpressing EGFP in hydrogel **2** stained with C<sub>18</sub>-Rho before (top) and after (bottom) UV irradiation. Insets in the bottom panel show images during UV irradiation. b) Movement locus of the bacteria for 126 s before gelation (left), after gelation (middle), and for 177 s after UV irradiation (right). c) Time courses of the accumulated migration distances of four representative bacteria in photoswitching experiments. UV irradiation for 30 s resulted in the two dotted lines for each bacterium. [gelator **2**] = 0.15 wt %. d) Schematic illustration of on/off switching of bacterial motion and rotation of microbead-tethered F<sub>1</sub>-ATPase by entanglement in the photoresponsive supramolecular hydrogel fibers (nanomesh).

the Supporting Information). This observation indicates that the light-responsive supramolecular hydrogel can perform off/on switching of the motor protein (Figure 5d).

#### Photo gel–sol patterning of the supramolecular hydrogel:

The phototriggered gel–sol transition provided us with a unique method for photopatterning of the hydrogel. Using an appropriate photomask, we photoirradiated limited areas

of supramolecular hydrogel prepared in a quartz cell. Typical examples are shown in Figure 6a. The photoirradiated area of the gel gradually turned into transparent sol due to the gel-to-sol phase transition. The sol areas produced by a 10 min of UV irradiation were more fluid and less viscous than the original gel, so that the sol area was replaced with an aqueous solution containing vitamin B<sub>12</sub> (Figure 6b).

Smaller photo gel–sol patterns were prepared by direct irradiation with the focal laser light (266 nm, see Figure S7 in the Supporting Information). A sol spot surrounded by gel was produced by spot irradiation with the laser light (<50  $\mu\text{m}$  diameter) in the flow-cell chamber (Figure 6c). The fluidity of the photogenerated sol in the small space (40–50  $\mu\text{m}$  in diameter) was evaluated by means of the Brownian motion of fluorescent microbeads. The Brownian motion of the microbeads in the solution phase and the sol phase of **2** stopped concurrently with gel formation. After laser irradiation for 0.125–0.25 s, motion of the seven microbeads in the focused spot restarted, whereas other beads outside the area of the laser beam never restarted moving. The motional velocity of the restarted beads was almost identical to that of beads in an aqueous solution (Figure 6d), that is, the area in the laser spot turned into the sol state. By laterally shifting the laser spot, we prepared various gel–sol patterns such as a dot pattern, continuous flow pathway, or characters

(Figure 6e). In the photoprepared dot pattern, we confirmed that the distance sufficient to maintain two independent sol spots was less than 10  $\mu\text{m}$  (Figure 6c), that is, a supramolecular gel wall 10  $\mu\text{m}$  in width acts as a barrier between the sol areas.

**Off/on switching of biomolecule movement by photoresponsive nanomesh in a restricted small area:** By using the

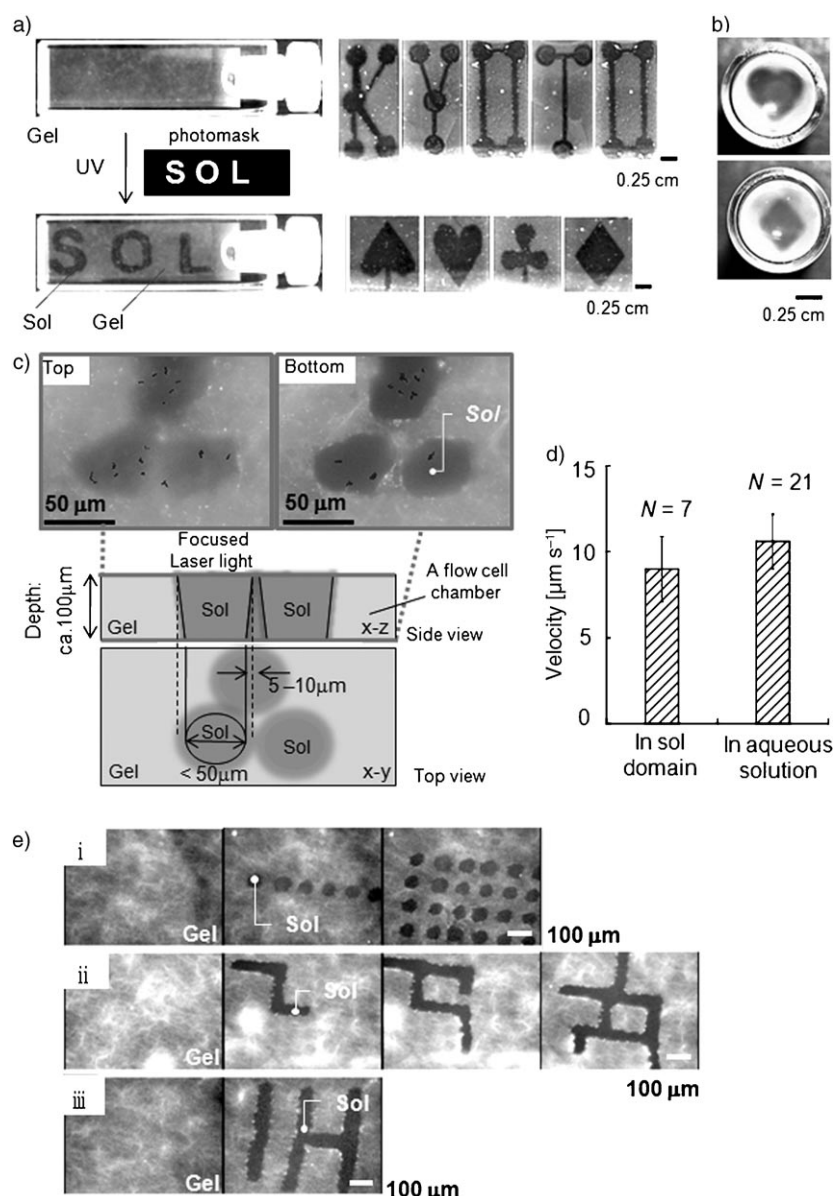


Figure 6. Photo gel-sol patterning of hydrogel **2**. a) Photographs of gel-sol patterning on the millimeter scale with man-made photomasks. b) Gel in which the photogenerated sol domains were replaced with vitamin B<sub>12</sub> solution. [Hydrogel **2**]=0.20 wt %, prepared in a quartz cell with light path length of 2 mm, ion-exchanged water). Irradiation for 10 min with xenon lamp. c) Photo gel-sol patterning on the micrometer scale. The dotted sol domains in hydrogel **2** with immobilized 250 nm fluorescent beads were fabricated with focused laser light (266 nm). The lines show Brownian motion of microbeads in the fabricated sol area at the bottom ( $z=0 \mu\text{m}$ ) and top ( $z \approx 100 \mu\text{m}$ ) surfaces. d) Comparison of mean velocities of the Brownian motion of beads in the sol domain and in the aqueous solution. e) Various photo gel-sol patterns prepared with the focused laser. i) Dots, ii) lines, and iii) character patterns "IH" was fabricated in hydrogel **2** with focused 266 nm laser light. See Supporting Information for color version of this figure.

above-mentioned gel-sol patterning in a flow-cell chamber, bacterial motion was spatially restricted to the sol spot produced by light. After all the bacteria were entrapped in supramolecular hydrogel **2**, irradiation with the focused laser spot 0.25 s yielded a sol 40  $\mu\text{m}$  in diameter. As shown in Figure 7a, the bacteria in the sol spot started moving again, whereas bacteria in the gel area that was not in the laser spot did not move. When a continuous sol pathway

was fabricated within the gel matrix by photo gel-sol patterning, we found that all the bacteria moved within the continuous path (Figure 7b). Importantly, no bacteria moved across the gel matrix, that is, the gel wall consisting of entangled gel meshes clearly acted as a barrier against bacterial movement.

In a similar manner, we switched the rotary motion of F<sub>1</sub>-ATPase in a small restricted area of the photoresponsive hydrogel mesh of **2** using focused laser light. After stopping F<sub>1</sub>-ATPase motion for more than 5 min in the hydrogel matrix, laser-light irradiation was performed for 2 s (1 s per shot,  $\times 2$ ) in a focused area (10–20  $\mu\text{m}$  diameter). Within two seconds, the F<sub>1</sub>-ATPase located in the photoirradiated spot started rotating again (see Movie S1 in the Supporting Information), whereas the other F<sub>1</sub>-ATPases out of the laser spot remained stopped (Figure 7c).<sup>[15]</sup>

## Conclusion

We have prepared biocompatible and photoresponsive supramolecular hydrogels based on partial rational design coupled with a combinatorial-library method. The sol state was produced within the gel matrix by using focused UV light with a spatial resolution of 1 mm to 10  $\mu\text{m}$ . We also found that the hydrogel is comprised of supramolecular meshes with void spaces of between 100 and 250 nm which can entrap nano-beads, microbead-tethered F<sub>1</sub>-

ATPase, and bacteria and suppress their movement through physical blocking by the gel meshes. The photo gel-to-sol phase transition induced the deformation of the supramolecular nanomeshes, so that the rotation of microbead-tethered F<sub>1</sub>-ATPase and bacterial motion were restarted in a spatially and temporally regulated manner. The present photoresponsive supramolecular hydrogel is promising as a unique biomaterial that can actively operate functions and spatially lo-

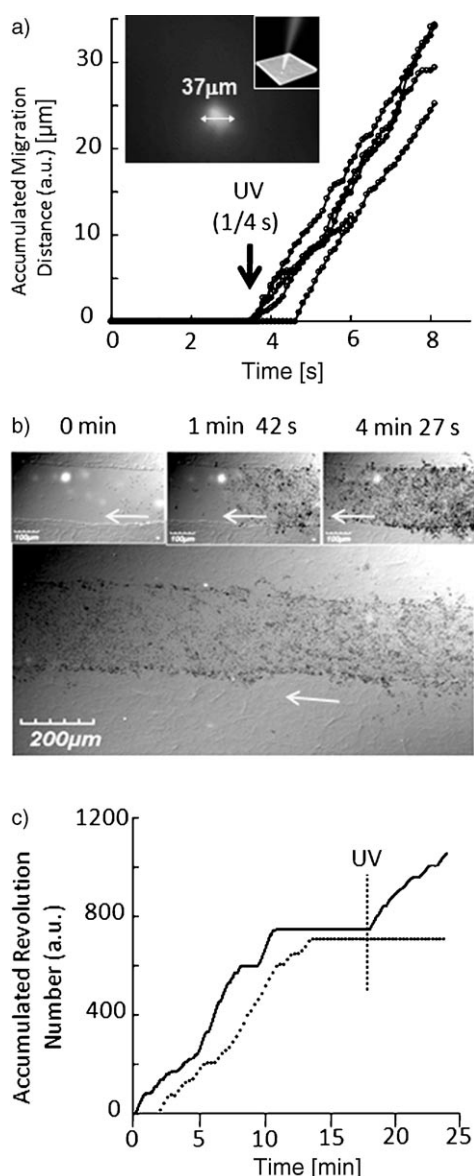


Figure 7. Off/on switching of bacterial movement and  $F_1$ -ATPase rotation in a spatially limited area. a) Time courses of the accumulated migration distances of five distinct bacteria before and after UV irradiation with focused 266 nm laser light (diameter of ca. 40  $\mu\text{m}$ , see inset). b) Bacterial movement in the sol flow path fabricated with focused laser light (266 nm). c) Time courses of accumulated numbers of rotations of  $F_1$ -ATPase molecules inside (solid line) and outside (dotted line) the laser-irradiated area (diameter of 10–20  $\mu\text{m}$ ).

calize bioactive molecules such as vitamins, proteins/enzymes, and live bacteria.

## Experimental Section

**General:** All gelators in this paper were synthesized according to Scheme S1 in the Supporting Information by our previously reported synthetic method.<sup>[16]</sup> Reagents for gelator synthesis were obtained from Kishida Chemical, Watanabe Chemical Industries, Wako, or TCI (Japan).

A mutant  $\alpha_3\beta_3\gamma$  subcomplex ( $\alpha$ -C193S,  $\beta$ -His-10 at N-terminus,  $\gamma$ -S107C/I210C) from a thermophilic *Bacillus* PS3 (referred to as  $F_1$ -ATPase) was expressed and purified as described elsewhere.<sup>[17]</sup> Streptavidin-coated magnetic beads (Seradyn; normally 0.73  $\mu\text{m}$ ) were sonicated to disperse them in a suspension and lightly centrifuged as described.<sup>[18]</sup>

**Gelation tests:** Synthesized glycolipid-based compounds were homogeneously dispersed with ion-exchanged water (0.05–2.0 wt %) by heating, and then left at rest for 12 h at room temperature. Gelation ability of each compound was checked visually by the vial-inversion method and then classified into four phase states: transparent gel, opaque gel, precipitate, and homogenous solution.

**Photoirradiation conditions for bulk gel–sol/sol–gel transition:** Hydrogel **2** (0.10–0.25 wt %, ion-exchanged water) prepared in a quartz cell (light path length 2 mm) was irradiated with UV light from a xenon lamp (USHIO, Optical Modulex, SX-UI500XQ) for at least 10 min below 15 °C. In the sol–gel transition of **2**, visible-light irradiation of the above-prepared sol containing a small amount of bromine was performed with a xenon lamp equipped with two filters (wavelength cutoffs >290 and >350 nm) for at least 10 min below 15 °C. This pseudo-photoreversible phenomenon could be repeated several times.

**Dynamic viscoelasticity measurements:** Dynamic viscoelasticities of hydrogel **2** (0.20 wt %) before and after UV irradiation with a xenon lamp for 1 h and of the reconstructed hydrogel after visible-light irradiation of the sol for 30 min in the presence of a small amount of bromine were measured with a plate–plate rheology instrument (DynAlyser DAR-100, Reologica). The measurement conditions were as follows: angular frequency range: 100–0.1  $\text{rads}^{-1}$ ; strain: 2% for the gel and the reconstructed gel sample and 0.5% for the sol sample (after UV irradiation to give gel **2**); parallel plate, 4 cm in diameter; gap distance: 1.2 mm; measurement temperature: 24 °C.

**Phase diagram for photoresponsive gel–sol transition:** Hydrogel **2** (0.20 wt %,  $\text{D}_2\text{O}$ ) was irradiated with UV light from a xenon lamp for irradiation times 0, 1, 3, 5, 7, 10, 20, and 30 min at 15 °C. The percentage gel:sol volume ratio of each sample was estimated by measuring the sol volume with a syringe and calculated as  $[\text{gel volume}/(\text{gel volume} + \text{sol volume})] \times 100$  (horizontal axis). Photoisomerization ratios of fumaric (*trans*) and maleic (*cis*) amide forms were estimated from the integrals of their peaks in  $^1\text{H}$  NMR spectra (JEOL-JNM-EX400, 400 MHz) of each sample, to which  $\text{CD}_3\text{OD}$  was added ( $\text{CD}_3\text{OD}/\text{D}_2\text{O}$  1/1 v/v) to prepare homogenous dispersed solutions. These ratios were calculated as  $(\text{fumaric})/(\text{fumaric} + \text{maleic}) \times 100$  (vertical axis). Each experiment was performed three times, and averages and error bar were calculated and plotted. In addition, byproducts were not observed in the  $^1\text{H}$  NMR spectra.

**TEM and SEM observations:** Carbon-coated copper grids were dipped into hydrogel **2**, the sol after gelling by UV irradiation with a xenon lamp for 30 min, or the reconstructed hydrogel **2**, which was prepared by visible-light irradiation of the sol in the presence of a small amount of bromine for 10 min with a xenon lamp attached with UV cut filters. They were dried under reduced pressure for 24 h at room temperature. TEM samples were stained with a 2 wt % aqueous solution of uranyl acetate. TEM observations were carried out with a JEOL JEM-2010 apparatus under 120 kV accelerating voltage. For SEM observation, the samples were coated by platinum vapor deposition (30 s). SEM images were obtained by using a Hitachi S-5000 with an acceleration voltage of 25 kV.  $[\text{Hydrogelator } \mathbf{2}] = 0.20 \text{ wt } \%$  (in ion-exchanged water).

**CLSM observations:** Hydrogel **2** and the sol after UV irradiation with a low-pressure Hg lamp for 1.5–3.5 min, stained with hydrophobic fluorescent dye (15  $\mu\text{m}$  octadecyl rhodamine B chloride, Molecular Probes), were observed with an Olympus FV1000, IX81 confocal laser scanning microscope.  $[\text{Hydrogelator } \mathbf{2}] = 0.10 \text{ wt } \%$  (in ion-exchanged water). The excitation wavelength was 543 nm.

**Observation of Brownian motion of microbeads in hydrogel **2**:** Heat-dispersed gelator **2** in ion-exchanged water containing 100, 250 nm fluorescent beads or 500, 1000 nm beads (Micromer-red F, POL) were dropped onto petri dish and left at rest for 3 h at room temperature. These samples were monitored by CLSM (Olympus FV1000) at an excitation laser wavelength of 543 nm in real time. Objective lens:  $\times 100$ .  $[\text{Hydrogel } \mathbf{2}] = 0.10 \text{ wt } \%$  (in ion-exchanged water).

**Release of biomolecules and microbeads from hydrogel 2:** Ion-exchanged water (400  $\mu\text{L}$ ) was added to hydrogel 2 (150  $\mu\text{L}$ , 0.10 wt %) containing vitamin B<sub>12</sub>, FITC-ConA (tetramer), or 100 or 250 nm fluorescent beads in a quartz cell. The overlying solution was monitored with a UV/Vis absorption spectrometer (Shimadzu UV-2550) in real time for 0–3 h. The time course of vitamin B<sub>12</sub> (0.20 mM) release was monitored by means of the absorption at 550 nm before UV irradiation, and at 410 nm after UV irradiation (410 nm was an isosbestic point of vitamin B<sub>12</sub> in aqueous solution before and after UV irradiation). The time course of FITC-ConA (0.14–0.27 mg/mL) release was monitored by means of the absorption at 492.5 nm before UV irradiation, and 421 nm after UV irradiation (421 nm was an isosbestic point of FITC-ConA in aqueous solution before and after UV irradiation). The time courses of release of monodisperse 100 or 250 nm fluorescent beads (micromer-red F, POL) were traced by means of the transmittance at 400 nm. In addition, we checked that the solubility of hydrogelator 2 in bulk solution was less than 1 vol % of gel over 5 h. Each experiment was repeated three times, and averages and error bars were calculated and plotted.

**Observation of bacteria entrapped in hydrogel:** A flow-cell chamber for observing bacterial movement was constructed from two uncoated glass plates (Matsunami; top 18  $\times$  18 mm, bottom 24  $\times$  32 mm) sandwiching two parallel strips of greasy paper as spacers.<sup>[14e]</sup> *Escherichia coli* BL21 (DE3) (Novagen) bacteria were suspended in the sol state of gelator 2 (0.15 wt %, ion-exchanged water) and immediately put into a flow chamber. We observed the movement of bacteria with a microscope by using the differential interference contrast (DIC) method and analyzed the locus and the accumulated distances of bacterial movement every 3 s (software Move-tr/2D 7.0, Library). To induce the photo gel–sol transition, a low-pressure mercury-vapor lamp (Ushio, UL0-6DQ) was located approximately 5 mm above the flow chamber and used to irradiate for 30 s. For the experiments with UV irradiation in limited areas, 266 nm laser light focused with an objective lens (100 $\times$ ) was used for 0.25 s.

**Observation of regulated F<sub>1</sub>-ATPase rotation in hydrogel:** Two parallel strips of greasy paper were placed on the Ni-patterned glass plate, and a quartz plate (10 mm  $\times$  10 mm, 1 mm thick) was put on the strips to form a flow chamber.<sup>[14e]</sup> F<sub>1</sub>-ATPase was immobilized on the glass plates in a flow chamber and modified with magnetic beads (normally 0.73  $\mu\text{m}$  in diameter) according to the method reported previously.<sup>[14e]</sup> All rotation assays were started by infusion of heat-dispersed gelator 2 (0.06–0.15 wt %) in MOPS buffer (50 mM 3-(*N*-morpholino)propanesulfonic acid/KOH (pH 7.1), 50 mM KCl) supplemented with 2 mM of Mg-ATP, and the rotating beads were observed as bright-field images at the single-molecule level. Video images were recorded and analyzed with custom software, and the accumulated numbers of revolutions were plotted every 0.033 s.<sup>[14e]</sup> In the UV irradiation experiments, a low-pressure mercury vapor lamp (Ushio, UL0-6DQ) was located approximately 5 mm above the flow chamber and used to irradiate for 1.5–3.5 min. For the experiments with UV irradiation in limited areas, 266 nm laser light focused with an objective lens (100 $\times$ ) was used for 2 s (1 s per shot,  $\times 2$ ).

**Photo gel–sol patterning on the microscale:** Hydrogel 2 (0.10 wt %, ion-exchanged water) containing 250 nm of fluorescent beads for visualization of the gel–sol pattern was prepared in a flow cell. By using a focused laser (266 nm, 0.125–0.25 s per shot), various line and character patterns were fabricated by connecting patterns of dots. At the bottom surface region of the flow cell, a sol domain of less than 50  $\mu\text{m}$  in diameter was formed, whereas in the upper surface region of the flow cell a sol domain of less than 50  $\pm$  (5–10)  $\mu\text{m}$  in diameter was confirmed by the Brownian motion of microbeads. The accumulated distances of Brownian motion of microbeads in the sol domain were analyzed with software (Move-tr/2D 7.0, Library).

## Acknowledgements

This research is partially supported by JST (PRESTO, Synthesis and Control). S.M. is a research fellow of the Japan Society for the Promotion of Science (JSPS).

- [1] a) D. B. Weibel, G. M. Whitesides, *Curr. Opin. Chem. Biol.* **2006**, *10*, 584–591; b) G. M. Whitesides, *Nature* **2006**, *442*, 368–373; c) D. B. Weibel, W. R. DiLuzio, G. M. Whitesides, *Nat. Rev. Microbiol.* **2007**, *5*, 209–218.
- [2] a) R. K. Soong, G. D. Bachand, H. P. Neves, A. G. Olkhovets, H. G. Craighead, C. D. Montemagno, *Science* **2000**, *290*, 1555–1558; b) T. O. Yeates, J. E. Padilla, *Curr. Opin. Struct. Biol.* **2002**, *12*, 464–470; c) S. G. Zhang, D. M. Marini, W. Hwang, S. Santoso, *Curr. Opin. Chem. Biol.* **2002**, *6*, 865–871; d) M. Sarikaya, C. Tamerler, A. K. Y. Jen, K. Schulten, F. Baneyx, *Nat. Mater.* **2003**, *2*, 577–585; e) N. C. Seeman, *Biochemistry* **2003**, *42*, 7259–7269; f) H. Hess, G. D. Bachand, V. Vogel, *Chem. Eur. J.* **2004**, *10*, 2110–2116; g) C. E. MacPhee, D. N. Woolfson, *Curr. Opin. Solid State Mater. Sci.* **2004**, *8*, 141–149; h) K. Rajagopal, J. P. Schneider, *Curr. Opin. Struct. Biol.* **2004**, *14*, 480–486; i) D. B. Weibel, P. Garstecki, D. Ryan, W. R. DiLuzio, M. Mayer, J. E. Seto, G. M. Whitesides, *Proc. Natl. Acad. Sci. USA* **2005**, *102*, 11963–11967; j) J. Xi, J. J. Schmidt, C. D. Montemagno, *Nat. Mater.* **2005**, *4*, 180–184; k) Y. Astier, H. Bayley, S. Howorka, *Curr. Opin. Chem. Biol.* **2005**, *9*, 576–584; l) Y. Hiratsuka, M. Miyata, T. Tada, T. Q. P. Uyeda, *Proc. Natl. Acad. Sci. USA* **2006**, *103*, 13618–13623; m) D. N. Woolfson, M. G. Ryadnov, *Curr. Opin. Chem. Biol.* **2006**, *10*, 559–567; n) L. Jaeger, A. Chworos, *Curr. Opin. Struct. Biol.* **2006**, *16*, 531–543.
- [3] For reviews, see: a) L. A. Estroff, A. D. Hamilton, *Chem. Rev.* **2004**, *104*, 1201–1218; b) N. M. Sangeetha, U. Maitra, *Chem. Soc. Rev.* **2005**, *34*, 821–836; c) M. De Loos, B. L. Feringa, J. H. van Esch, *Eur. J. Org. Chem.* **2005**, *17*, 3615–3631.
- [4] a) S. Kiyonaka, K. Sada, I. Yoshimura, S. Shinkai, N. Kato, I. Hamachi, *Nat. Mater.* **2004**, *3*, 58–64; b) M. P. Lutolf, J. A. Hubbell, *Nat. Biotechnol.* **2005**, *23*, 47–55; c) R. V. Ulijn, *J. Mater. Chem.* **2006**, *16*, 2217–2225; d) R. V. Ulijn, N. Bibi, V. Jayawarna, P. D. Thornton, S. J. Todd, R. J. Mart, A. M. Smith, J. E. Gough, *Materials Today* **2007**, *10*, 40–48.
- [5] a) S. Zhang, *Nat. Biotechnol.* **2003**, *21*, 1171–1178; b) G. A. Silva, C. Czeisler, K. L. Niece, E. Beniash, D. A. Harrington, J. A. Kessler, S. I. Stupp, *Science* **2004**, *303*, 1352–1355.
- [6] Examples of pH-responsive supramolecular hydrogels: a) S. R. Haines, R. G. Harrison, *Chem. Commun.* **2002**, 2846–2847; b) S. Kiyonaka, S. L. Zhou, I. Hamachi, *Supramol. Chem.* **2003**, *15*, 521–528; c) S. L. Zhou, S. Matsumoto, H. D. Tian, H. Yamane, A. Ojida, S. Kiyonaka, I. Hamachi, *Chem. Eur. J.* **2005**, *11*, 1130–1136; d) D. Khatua, R. Maitib, J. Dey, *Chem. Commun.* **2006**, 4903–4905.
- [7] a) Z. M. Yang, H. W. Gu, D. G. Fu, P. Gao, J. K. Lam, B. Xu, *Adv. Mater.* **2004**, *16*, 1440–1444; b) Z. Yang, G. Liang, L. Wang, B. Xu, *J. Am. Chem. Soc.* **2006**, *128*, 3038–3043; c) Z. Yang, B. Xu, *Adv. Mater.* **2006**, *18*, 3043–3046; d) P. K. Vemula, J. Li, G. John, *J. Am. Chem. Soc.* **2006**, *128*, 8932–8938; e) S. Toledano, R. J. Williams, V. Jayawarna, R. V. Ulijn, *J. Am. Chem. Soc.* **2006**, *128*, 1070–1071; f) Z. Yang, G. Liang, B. Xu, *Soft Matter* **2007**, *3*, 515–520; g) Z. Yang, G. Liang, M. Ma, Y. Gao, B. Xu, *Small* **2007**, *3*, 558–562; h) Z. Yang, P.-L. Ho, G. Liang, K. H. Chow, Q. Wang, Y. Cao, Z. Guo, B. Xu, *J. Am. Chem. Soc.* **2007**, *129*, 266–267.
- [8] a) Y. Zhang, H. Gu, Z. Yang, B. Xu, *J. Am. Chem. Soc.* **2003**, *125*, 13680–13681; b) T. Ogoshi, Y. Takashima, H. Yamaguchi, A. Harada, *J. Am. Chem. Soc.* **2007**, *129*, 4878–4879.
- [9] a) K. Murata, M. Aoki, T. Suzuki, T. Harada, H. Kawabata, T. Komori, F. Ohseto, K. Ueda, S. Shinkai, *J. Am. Chem. Soc.* **1994**, *116*, 6664–6676; b) L. N. Lucas, J. van Esch, R. M. Kellogg, B. L. Feringa, *Chem. Commun.* **2001**, 759–760; c) S. Yagai, T. Karatsu, A. Kitamura, *Chem. Eur. J.* **2005**, *11*, 4054–4063; d) J. J. D. De Jong, P. R. Hania, A. Pugzlys, L. N. Lucas, M. De Loos, R. M. Kellogg, B. L. Feringa, K. Duppen, J. H. van Esch, *Angew. Chem.* **2005**, *117*, 2425–2428; *Angew. Chem. Int. Ed.* **2005**, *44*, 2373–2376; e) H. Sakai, Y. Orihara, H. Kodashima, A. Matsumura, T. Ohkubo, K. Tsuchiya, M. Abe, *J. Am. Chem. Soc.* **2005**, *127*, 13454–13455; f) A. M. Ketner, R. Kumar, T. S. Davies, P. W. Elder, S. R. Raghavan, *J. Am. Chem. Soc.* **2007**, *129*, 1553–1559.

- [10] a) M. Irie, D. Kunwachakun, *Macromolecules* **1986**, *19*, 2476–2480; b) A. Mamada, T. Tanaka, D. Kungwachakun, M. Irie, *Macromolecules* **1990**, *23*, 1517–1519; c) L. Frkanec, M. Jokic, J. Makarevic, K. Wolsperger, M. Zinic, *J. Am. Chem. Soc.* **2002**, *124*, 9716–9717; d) T. Hirakura, Y. Nomura, Y. Aoyama, K. Akiyoshi, *Biomacromolecules* **2004**, *5*, 1804–1809; e) L. A. Haines, K. Rajagopal, B. Ozbas, D. A. Salick, D. J. Pochan, J. P. Schneider, *J. Am. Chem. Soc.* **2005**, *127*, 17025–17029; f) I. Tomatsu, A. Hashidzume, A. Harada, *Macromolecules* **2005**, *38*, 5223–5227.
- [11] a) S. Shinkai, T. Ogawa, T. Nakaji, Y. Kusano, O. Manabe, *Tetrahedron Lett.* **1979**, *20*, 4569–4572; b) S. Shinkai, *Pure Appl. Chem.* **1987**, *59*, 425–430; c) N. Koumura, R. W. J. Zijlstra, R. A. van Delzen, N. Harada, B. L. Feringa, *Nature* **1999**, *401*, 152–155; d) V. Balzani, A. Credi, F. M. Raymo, J. F. Stoddart, *Angew. Chem. Int. Ed.* **2000**, *39*, 3349–3391; e) M. Irie, *Chem. Rev.* **2000**, *100*, 1685–1716; f) A. M. Brouwer, C. Frochot, F. G. Gatti, D. A. Leigh, L. Mottier, F. Paolucci, S. Roffia, G. W. H. Wurpel, *Science* **2001**, *291*, 2124–2128; g) F. M. Raymo, *Adv. Mater.* **2002**, *14*, 401–414; h) J. V. Hernandez, E. R. Kay, D. A. Leigh, *Science* **2004**, *306*, 1532–1537; i) K. Kinbara, T. Aida, *Chem. Rev.* **2005**, *105*, 1377–1400; j) J.-M. Lehn, *Chem. Eur. J.* **2006**, *12*, 5910–5915; k) W. R. Browne, B. L. Feringa, *Nat. Nanotechnol.* **2006**, *1*, 25–35; l) G. Mayer, A. Heckel, *Angew. Chem.* **2006**, *118*, 5020–5042; *Angew. Chem. Int. Ed.* **2006**, *45*, 4900–4921; m) E. R. Kay, D. A. Leigh, F. Zerbetto, *Angew. Chem.* **2007**, *119*, 72–196; *Angew. Chem. Int. Ed.* **2007**, *46*, 72–191; n) V. Balzani, A. Credi, M. Venturi, *NanoToday* **2007**, *2*, 18; o) S. Saha, J. F. Stoddart, *Chem. Soc. Rev.* **2007**, *36*, 77–92; p) A. Credi, H. Tian, *Adv. Funct. Mater.* **2007**, *17*, 679–682.
- [12] a) T. G. Mason, D. A. Weitz, *Phys. Rev. Lett.* **1995**, *74*, 1250–1253; b) J. C. Crocker, M. T. Valentine, E. R. Weeks, T. Gisler, P. D. Kaplan, A. G. Yodh, D. A. Weitz, *Phys. Rev. Lett.* **2000**, *85*, 888–891; c) A. P. Nowak, V. Breedveld, L. Pakstis, B. Ozbas, D. J. Pine, D. Pochan, T. J. Deming, *Nature* **2002**, *417*, 424–428.
- [13] S. Yamaguchi, S. Matsumoto, K. Ishizuka, Y. Iko, K. V. Tabata, H. F. Arata, H. Fujita, H. Noji, I. Hamachi, *Chem. Eur. J.* **2008**, *14*, 1891–1896.
- [14] a) H. Noji, R. Yasuda, M. Yoshida, K. Kinoshita Jr., *Nature* **1997**, *386*, 299–302; b) R. Yasuda, H. Noji, M. Yoshida, K. Kinoshita Jr., H. Itoh, *Nature* **2001**, *410*, 898–904; c) Y. Hirono-Hara, H. Noji, M. Nishiura, E. Muneyuki, K. Y. Hara, R. Yasuda, K. Kinoshita Jr., M. Yoshida, *Proc. Natl. Acad. Sci. USA* **2001**, *98*, 13649–13654; d) H. Itoh, A. Takahashi, K. Adachi, H. Noji, R. Yasuda, M. Yoshida, K. Kinoshita Jr., *Nature* **2004**, *427*, 465–468; e) Y. Hirono-Hara, K. Ishizuka, K. Kinoshita Jr., M. Yoshida, H. Noji, *Proc. Natl. Acad. Sci. USA* **2005**, *102*, 4288–4293.
- [15] To examine the heating effect of light irradiation, a control experiment with 0.35 wt % of thermally responsive hydrogel GalNAc-sucglu(*O*-methyl-cyc-pentyl)<sub>2</sub> (**3**)<sup>[16]</sup> instead of photoresponsive hydrogel **2** was conducted. To make this control system absorb the laser light similarly to hydrogel **2**, fumaric acid was mixed with hydrogel **3** in equimolar concentration to gelator **2** (1.5 mM). Rotation of the microbead attached to F<sub>1</sub>-ATPase in hydrogel **3** including fumaric acid was stopped by gelation. However, during subsequent laser irradiation, the microbeads remained motionless (data not shown). Since the *T*<sub>g</sub> of hydrogel **3** (48 ± 2 °C) is lower than that of hydrogel **2** ((63 ± 3) °C), the heating effect of light irradiation can be ruled out as the main factor causing restart of microbead rotation.
- [16] S. Kiyonaka, S. Shinkai, I. Hamachi, *Chem. Eur. J.* **2003**, *9*, 976–983.
- [17] D. Bald, H. Noji, M. Yoshida, Y. Hirono-Hara, T. Hisabori, *J. Biol. Chem.* **2001**, *276*, 39505–39507.
- [18] H. Itoh, A. Takahashi, K. Adachi, H. Noji, R. Yasuda, M. Yoshida, K. Kinoshita Jr., *Nature* **2004**, *427*, 465–468.

Received: December 4, 2007  
Published online: March 11, 2008